LA-UR- 09-01069

Approved for public release; distribution is unlimited.

Title:	Measurement and simulation of jet mass caused by a high-aspect ratio perturbation
Author(s):	Paul Keiter, Jim Elliott, Brent Blue, James Cooley, John Edwards, George Kyrala, Harry Robey, Brian Spears, Doug Wilson
Intended for:	Submission to Physics of Plasmas Journal

Los Alamos
NATIONAL LABORATORY
EST. 1943

Form 836 (7/06)

Measurement and simulation of jet mass caused by a high-aspect ratio perturbation

Paul Keiter[1], Jim Elliott[2], Brent Blue[2], James Cooley[1], John Edwards[2], George Kyrala[1], Harry Robey[2], Brian Spears[2], Doug Wilson[1]

[1] Los Alamos National Laboratory, Los Alamos, NM 87545
[2] Lawrence Livermore National Laboratory, Livermore, CA

Abstract

Inertial confinement fusion (ICF) capsule performance can be negatively impacted by the presence of hydrodynamic instabilities. To perform a gas fill on an ICF capsule current plans involve drilling a small hole and inserting a fill tube to inject the gas mixture into the capsule. This introduces a perturbation on the capsule, which can seed hydrodynamic instabilities. The small hole can cause jetting of the shell material into the gas, which might adversely affect the capsule performance. We have performed simulations and experiments to study the hydrodynamic evolution of jets from high-aspect ratio holes, such as the fill tube hole. Although simulations using cold materials over predict the amount of mass in the jet, when a reasonable amount of preheat (< 1 eV) is introduced, the simulations are in better agreement with the experiment.

Introduction

Current ICF ignition baseline capsule designs for the National Ignition Facility (NIF) use a graded-doped beryllium (Be) ablator.[1,2] The Be ablator is non-permeable and therefore, filling of the capsule with a deuterium-tritium (DT) gas mixture cannot be accomplished by immersing the capsule in DT gas and allowing the gas to diffuse through the ablator. There are few options for filling a capsule with a Be-ablator,[3]

however we will focus on only one method, the fill tube. A small hole is drilled into the capsule and a thin glass or polyimide fill tube is attached to the capsule over this hole. Both the hole and fill tube will introduce perturbations to the system. The fill tube produces a shadowing effect which can introduce a perturbation due to the non-uniform illumination of the capsule. When the shocks are launched in the capsules, the lower density material that is in the hole will be pushed out, forming a jet.[4] It is important to understand the evolution of these defects to predict what effect it may have on the performance of an ICF capsule.

There has been some previous work that has looked at the different aspects of the fill tube induced perturbations. Bennett *et al*[5] measured the mass of the fill tube bump caused by the shadowing effect and compared their results to simulations. Langer *et al*[6] compare simulations to experimental results where indirectly driven capsules have a manufactured perturbation initially. They observe the emission of material injected into the capsule but do not measure the mass of the jet created by their perturbations.

There has been much previous work studying the evolution of jets[7,8]. However, most of this work centers on small aspect ratio (< 2) holes. Holes of interest for ICF capsules have much larger aspect ratios (>10). The experimental results presented here provide data on such holes. Purpose of the experiments is to provide data for testing of models for high aspect ratio holes.

Due to the complications of fabricating, diagnosing and simulating an ICF Be capsule implosion in 3-dimensions (3-D), these experiments were performed in a planar geometry. Simulation results are then compared to the experimental results to determine how well the simulations can predict the amount of mass included in the jet. These

experiments allow us to test the codes ability to model these high-aspect ratio jets without the complications due to a 3-D geometry.

Experimental Configuration

These experiments are performed at the OMEGA laser facility.[9] A cartoon of the experimental package is shown in Figure 1. The ablator is nominally 100 microns thick and composed of Be doped with 3% by atom of copper. The BeCu washer is nominally 200 microns thick and composed of the same Be doped with 3% by atom Cu as the BeCu ablator. Centered in the washer is a hole whose dimensions were chosen in the range of 20 microns in diameter to 100 microns in diameter. The results presented in this paper will concentrate on 40 and 50 micron diameter holes. After the BeCu washer, is a foam region into which the BeCu jet propagates. This foam is carbon resorcinol formaldehyde (CRF) and is nominally 1.2 mm long and 1.2 mm in diameter with a nominal density of 50 mg/cc.

Fifteen laser beams nominally deliver 7.5 kJ of energy to the *Hohlraum*, which creates a temperature drive. The temperature drive is characterized by the Dante[10] diagnostic and has a peak temperature of roughly 200 eV. The temperature drive irradiates the drive-side of the Be ablator and launches a shock in the Be. The shock ejects some of the Be ablator down through the hole and this material forms the head or cap of the jet. The shock also travels through the Be washer and pushes material into the vacuum region of the washer. The material collides on axis and is the jetted into the foam, forming the stem of the jet.

A foil irradiated by laser beams was used as an x-ray source to produce radiographs of the jet evolution as a function of time. Both area backlighters and point-projection backlighters were used in the experiments. The area backlighter consisted of a Cl foil which produced x-ray radiation primarily at 2.8 keV and was used for the smaller diameter holes. The radiographs were recorded using an x-ray framing camera with a micro-channel plate. The point-projection configuration consisted of a Sc foil which produced x-ray radiation primarily at 4.3 keV and was used for the larger diameter holes. In this configuration the images were recorded directly onto film, either Kodak Direct Exposure Film (DEF) or AGFA D7.

Determination of Jet Mass

In order to determine the mass of the jets from the radiographs, care must be taken in the analysis. Besides the desired signal, there can be other contributions (*e.g.* film fog) to the signal measured on a piece of x-ray film, such that the total signal on the film (S_{film}) can be represented by contributions from the desired source and from sources of noise, such as the fog: $S_{film}=S_{source}+S_{background}$. Before one can determine the transmission of the film, the contribution due to the noise sources must be removed. This is typically done by examining a region of the film where the transmission due to the desired source should be zero. Therefore, any signal that is present should only be due to sources of noise. Once this subtraction has been performed, then the film signal can be converted into a transmission in order to determine the mass of the observed jets.

To determine the jet mass, we have made the following assumptions. First the transmission of the radiograph is equal to the transmission of the foam and the

transmission of the jet; $T_{tot}=T_{foam}T_{jet}$. Therefore we can determine the transmission of the jet by dividing out the transmission of the foam. Thus, $T_{jet}= T_{tot}/T_{foam}$. Also, recall that $T_{jet}=I/I_0=\exp(-\mu_{BeCu}\rho_{jet}r_{jet})$, where I is the measured intensity through the object I_0 is the unattenuated intensity from the backlighter, μ_{BeCu} is the mass absorption constant for the BeCu material, ρ_{jet} is the density of the jet and r_{jet} is the radius of the jet. Thus $\ln(T_{jet})=-\mu_{BeCu}\rho_{jet}r_{jet}$. This can be rewritten as $\ln(T_{jet})=-\mu_{BeCu}r_{jet}M_{jet}/V_{jet}$, where M_{jet} is the mas of the jet and V_{jet} is the volume of the jet. Therefore the mass of the jet can be determined using the following relation: $M_{jet}= -\ln(T_{jet})V_{jet}/\mu_{BeCu}r_{jet}$. The volume of the jet can be written as $V_{jet} = A_{jet}r_{jet}$, where r is the thickness and A is the area of the jet. At this point we note that in determining values from the radiograph this formula is applied to each pixel and therefore A_{jet} is essentially the pixel area. The mass can be rewritten as $M_{jet}= -\ln(T_{jet})A_{jet}/\mu_{BeCu}$. Both the transmission and the pixel area are measured quantities while the mass absorption coefficient is found in the NIST photon cross sections database.[11]

As stated previously, some of the x-ray data was obtained on AGFA D7 film. Although there is no absolute calibration for exposure levels of the D7 film, relative calibrations of D7 to Kodak DEF film have been performed[12,13] and can be used to convert the exposure levels of the D7 film to intensities in order to determine the transmission.

HYDRA Simulations

The simulations were conducted using the HYDRA[14] code in two dimensional, RZ geometry, with the fill tube on axis. The radiation transport was treated in the

diffusion approximation using 15 energy groups. The equations of state (EOS) for all materials used were from a combined analytic / Thomas-Fermi EOS which uses a modified Cowan model for the ion EOS, and uses a scaled Thomas-Fermi table for the electron EOS.

The initial setup of the computation model is shown, schematically, in Figure 2. The physical dimensions of the model are 0.0 cm <= R <= 0.025 cm and −0.1 cm <= Z <= 0.6 cm. From −0.1 cm <= Z <= 0.0 cm is carbonized resorcinol formaldehyde (CRF) at an initial temperature of $T_0 = 10^{-3}$ eV and an initial density of $\rho_0 = 0.05$ g/cm^3. From 0.0 cm <= Z <= 0.03 cm is copper-doped beryllium (3% copper by atom) at an initial temperature of $T_0 = T_{ph}$ (where T_{ph} is the pre-heat temperature as will be discussed below) and initial density of $\rho_0 = 1.848$ g/cm^3.

A cylindrically symmetric cavity of dimension 0.0 cm <= R <= 0.0025 cm by 0.0 cm <= Z <= 0.02 cm in the copper-doped beryllium is filled with helium at an initial temperature of $T_0 = 10^{-3}$ eV and an initial density of $\rho_0 = 10^{-4}$ g/cm^3. From 0.03 cm <= Z <= 0.0308 cm is parylene-N at an initial temperature of $T_0 = 10^{-3}$ eV and an initial density of $\rho_0 = 1.11$ g/cm^3. This serves as an ablator. Finally, from 0.0308 cm <= Z <= 0.6 cm is helium at an initial temperature of $T_0 = 10^{-3}$ eV and an initial density of $\rho_0 = 1.25 \times 10^{-4}$ g/cm^3. The helium is not present in the experiment, but is used in the simulations to avoid zone-mass discontinuities.

A Planckian temperature source is incident from Z = 0.6 cm. The source profile was scaled to match the experimental location of the pedestal at t = 15 ns.

Simulation Results Compared to Experiment

Using the as-shot drive conditions, three metrics from the experimental results were used to "grade" the results of the computational model. These metrics are the mass of the jet, the height of the jet and the location of the shock wave ahead of the pedestal. As previously stated, the simulation matches the position of the pedestal well since the temperature drive was scaled to match this position. The simulation also matches the position of the shock front to within 10%. However, the simulation over predicts both the jet mass and the jet height.

The simulations were studied in detail to determine why they disagreed with the experiment on the hydrodynamics of the jet evolution and not the larger scale hydrodynamics. One of the parameters studied was the pre-heat temperature of the Cu-doped Be ablator and washer.

Although the amount of preheat is not experimentally measured, pre-heat from the M-band emission of the gold *Hohlraum* is a common occurrence. It should also be noted that experiments were performed by R.E. Olson et al[15] to study indirectly-driven ICF ablator materials. In these experiments 75 microns thick of 0.9% Cu-doped Be was examined. It was found that the experimentally measured shock temperature and shock velocity data were better matched when assuming the ablator material was preheated to a level on the order of 4 eV. Based on this previous experimental evidence, the pre-heat in the simulations was varied from 0 eV to 1 eV.

Effect of Preheat in Simulations

As stated before, three metrics from the experimental results were used to "grade" the results of the computational model. These metrics are the mass of the jet, the height of the jet and the location of the shock wave ahead of the pedestal. The results from the simulations where the pre-heat was varied from 0-1 eV for each of these metrics at time t ~ 15 ns are shown in Figure 3, Figure 4 and Figure 5 respectively.

As mentioned above, the height of the beryllium pedestal observed in simulations agrees with the experimental results because the temperature source was chosen to insure that agreement and also because the time at which the simulation was sampled was chosen to maximize agreement of the height of the beryllium pedestal between simulation and experiment. The height of the shock ahead of the beryllium pedestal observed in the simulation agrees with the experimental results to within ten percent for all values of T_{ph}. This shows that the bulk hydrodynamics are not affected by the pre-heat.

When the copper-doped beryllium is pre-heated and melts, it flows into the cavity thereby closing it. Figure 6 and Figure 7 show how much copper-doped beryllium is preheated has flowed into the hole and the radius of the hole at the time at which the shock due to the temperature source arrives at the bottom of the cavity, respectively. The greater the pre-heat temperature, the smaller the cavity through which the shock due to the temperature source travels and, in general, the less massive and spatially smaller the jet.

Generally, Figure 3 shows the mass of the beryllium jet decreasing as initial temperature of the copper doped beryllium increases. However, there is a "shoulder" in

this trend that starts at $T_{ph} = 0.3$ eV and ends at $T_{ph} = 0.4$ eV. This shoulder is an artifact of the method used to determine the mass of the jet.

Figure 8 shows four simulations which give rise to the M_{jet} shoulder. The algorithm used to define the jet is: all copper-doped beryllium beyond the pedestal, or above the cut off boundary, is part of the jet (see horizontal dashed lines in Figure 8). As the initial temperature of the copper-doped beryllium is increased, the base of the jet (the region of highest beryllium density) widens. Also as the initial temperature of the copper doped beryllium is increased, the pedestal becomes less smooth (see the sections circled in Fig. 11). These two effects compete. As the base of the jet widens, the mass of the jet increases. As the pedestal smoothness decreases, the cut off boundary of the jet rises and the mass of the jet decreases. Eventually, the decrease in pedestal smoothness effect dominates and the trend of decreasing jet mass is resumed.

The overall trend of decreasing jet mass with increasing initial temperature of the copper-doped beryllium is a real and physical effect as will be discussed below.

As with the mass of the jet, the general trend is that the height of the jet decreases as the initial temperature of the copper-doped beryllium increases. However, Figure 4 shows that there is a "peak" in the jet height with a maximum at $T_{ph} = 0.6$ eV. Figure 8 shows the change in the shape and height of the jet as a function of T_{ph}.

The contraction of the cavity gives rise to supersonic pressure waves which propagate through the low-density medium. This interaction of the shock due to the temperature source and the pressure wave in the cavity due to the flow of the copper-doped beryllium into the cavity greatly affects the spatial size and shape of the jet. The speed of the pressure waves in the cavity depends on the speed with which the copper-

doped beryllium flows into the cavity, which in turn depends on its initial temperature. For lower values of T_{ph} the pressure wave in the cavity does not travel far by the time the shock due to the temperature source completes its transit through the cavity. For higher values of T_{ph} the pressure wave in the cavity travels to the axis of symmetry (R = 0.0 cm) by the time the shock due to the temperature source completes its transit through the cavity. For even higher values of T_{ph} the pressure wave in the cavity has been reflected at the axis of symmetry (R = 0.0 cm) and is traveling back towards the wall of the cavity by the time the shock due to the temperature source completes its transit through the cavity.

For initial temperatures $T_{ph} <= 0.4$ eV the pressure waves are slow and weak and have little interaction with the shock due to the temperature source and the spatial size of the jet decreases because the cavity size decreases.

For larger initial temperatures 0.5 eV $<= T_{ph} <=$ 0.6 eV pressure wave velocities are less than zero (i.e. moving towards R = 0.0 cm) and interact with the shock from the temperature source to cause spatially larger jets. At T_{ph} = 0.6 eV the pressure wave just reaches the axis of the cavity when the shock wave due to the temperature source reaches the top of the cavity and the jet reaches its maximum spatial extent.

For $T_{ph} > 0.6$ eV the pressure wave in the cavity has reached the axis, been reflected and is traveling back towards the wall of the cavity when the shock wave due to the temperature source reaches the top of the cavity and the spatial extent of the jet begins to decrease.

The pressure wave in the cavity acts to forward focus the jet. When the pressure wave is far from the axis during the shock transit through the cavity (i.e. for $T_{ph} < 0.6$ eV)

or when the pressure wave has been reflected (i.e. for $T_{ph} > 0.6$ eV) the forward focusing is less than when the pressure wave is closest to the axis (i.e. when $T_{ph} = 6 \times 10^{-4}$ KeV).

As demonstrated above, some pre-heating of the copper-doped beryllium closes the cavity which, in general, leads to less massive and spatially smaller jets. If the shock is delayed until the cavity is nearly filled there is almost complete suppression of the jet and a uniform shock front is observed. This is shown in Figure 9 where the copper-doped beryllium was pre-heated to a temperature of $T_{ph} = 0.9$ eV and the temperature source was delayed by 2.1 ns.

Simulations with material of higher density filling the cavity in the copper-doped beryllium show similar results. Specifically, at about 13 ns after application of the temperature source, simulations of a pre-heated copper-doped beryllium and delayed temperature source yielded a 94% reduction in the mass of the jet as compared to a zero pre-heat, no delay simulation.

A comparison of the two simulated radiographs in Figure 10 shows two drastically different jets. The preheated jet appears to have a smaller jet head than the non-heated jet. This is consistent with the simulations, since the hole becomes smaller in the preheated case before the initial shock, which pushes the ablator material in front of it, reaches the hole. Also, the shape of this jet head is different in both cases. In the non-heated case, the head is relatively flat across the top and then drops off quickly. In the preheated case, the head is flat for a much smaller portion and then it gradually slops back until it meets the pedestal material. This shape is most likely due to the gradient density in the hole which cause the shock and hence the material being pushed by the shock to propagate at a difference velocity across the diameter of the hole.

There may be additional benefits to pre-heating, namely any surface roughness would be smoothed out by the surface tension of the now liquid copper doped beryllium. This would occur in a fashion similar to the closing of the cavity demonstrated above. Unfortunately, HYDRA is not able to easily simulate the effects of surface tension. Also any crystalline in the copper doped beryllium would vanish, leaving a more uniform medium through which any shock waves would travel.

The shock and pedestal positions shown in Figure 11 does not help limit the acceptable preheat levels since they match the experiment well within the error bars. However, the simulated jet height agrees with the data in the range of 0.3-0.4 eV and 0.7–1.0 eV. The jet mass (Figure 13) helps to constrain the pre-heat by observing the simulated jet mass does not agree with the experimentally determined jet mass until the preheat level is over 0.1 eV. Figure 12 shows that the simulated pedestal position matches the experimental measurements best for pre-heat levels less than 0.4 eV.

When the simulations are compared to these experimental measurements, a consistent picture is formed. The simulations using 0.4 eV of pre-heat agree with three experimentally measured figures of merit: the jet mass, the jet height and the pedestal position and timing. In this way we are able to constraint the results of the simulations from the experiment.

Conclusions

The jet mass and jet height from high aspect ratio (4-5) has been experimentally investigated. Simulations with no preheat included over predict the amount of mass observed in the jet and the jet height while matching the pedestal position. However, a

small amount of preheat (< 1 eV) added to the simulation brings both the jet mass and the jet height into agreement with the experiment and maintains the agreement with the pedestal.

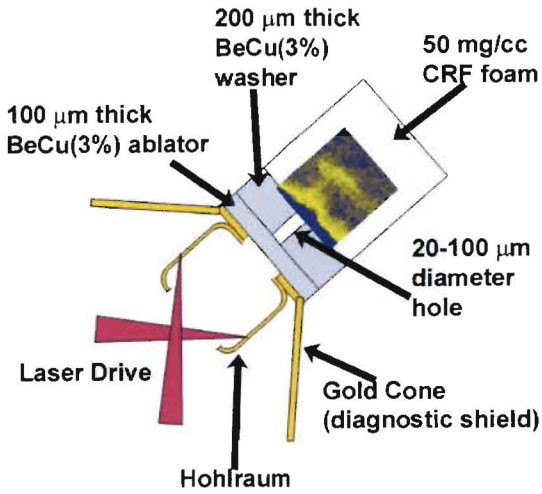
200 μm thick
BeCu(3%)
washer
50 mg/cc
CRF foam
100 μm thick
BeCu(3%) ablator
20-100 μm
diameter
hole
Laser Drive
Gold Cone
(diagnostic shield)
Hohlraum

Figure 1

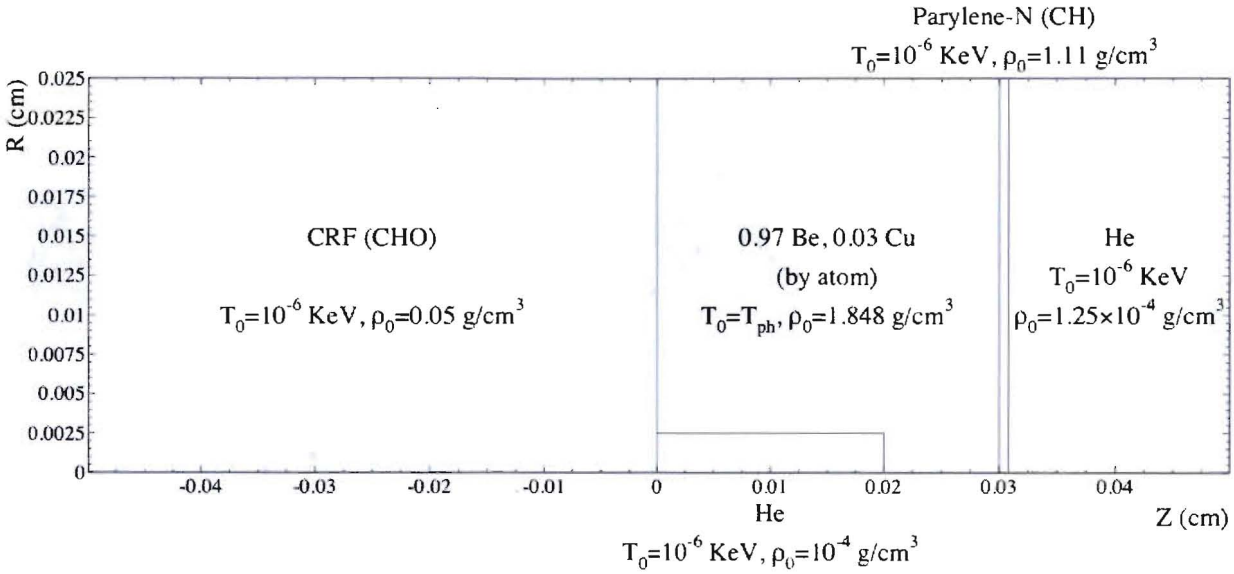
Parylene-N (CH)
$T_0=10^{-6}$ KeV, $\rho_0=1.11$ g/cm^3
R (cm)
0.025
0.0225
0.02
0.0175
0.015
0.0125
0.01
0.0075
0.005
0.0025
0
CRF (CHO)
$T_0=10^{-6}$ KeV, $\rho_0=0.05$ g/cm^3
0.97 Be, 0.03 Cu
(by atom)
$T_0=T_{ph}$, $\rho_0=1.848$ g/cm^3
He
$T_0=10^{-6}$ KeV
$\rho_0=1.25\times10^{-4}$ g/cm^3
-0.04
-0.03
-0.02
-0.01
0
0.01
0.02
0.03
0.04
Z (cm)
He
$T_0=10^{-6}$ KeV, $\rho_0=10^{-4}$ g/cm^3

Figure 2

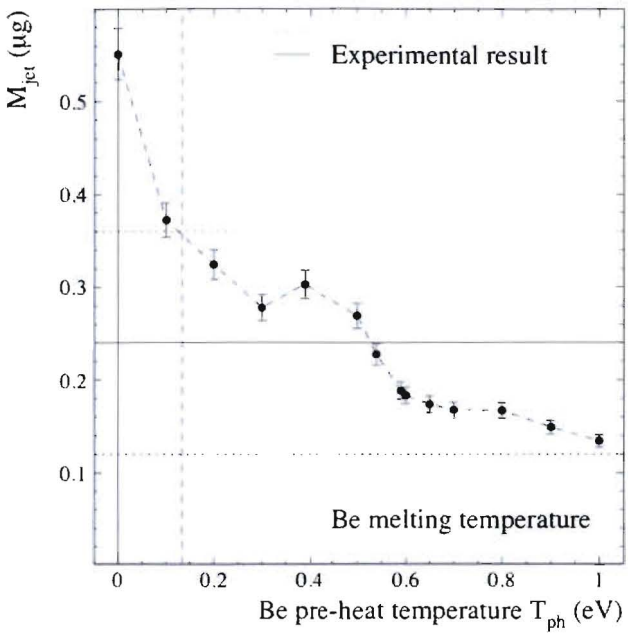
Experimental result
Be melting temperature
M_{jet} (μg)
0.5
0.4
0.3
0.2
0.1
0
0.2
0.4
0.6
0.8
1
Be pre-heat temperature T_{ph} (eV)

Figure 3

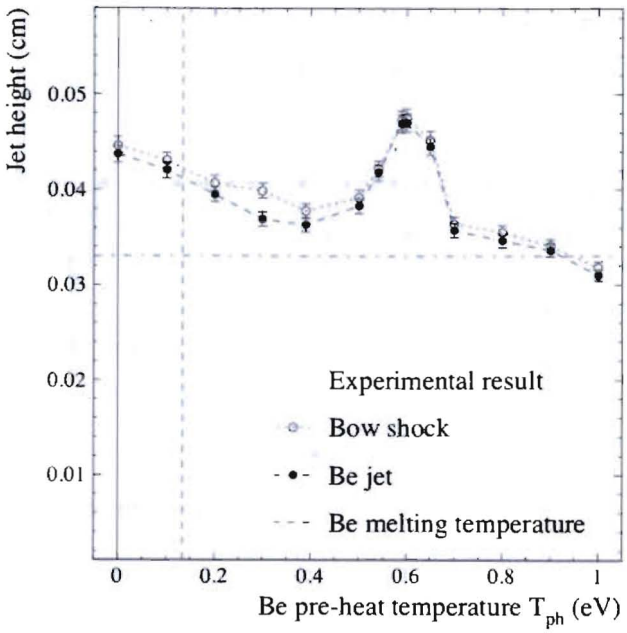
Jet height (cm)
0.05
0.04
0.03
0.02
0.01
0
0.2
0.4
0.6
0.8
1
Be pre-heat temperature T_{ph} (eV)
Experimental result
Bow shock
Be jet
Be melting temperature

Figure 4

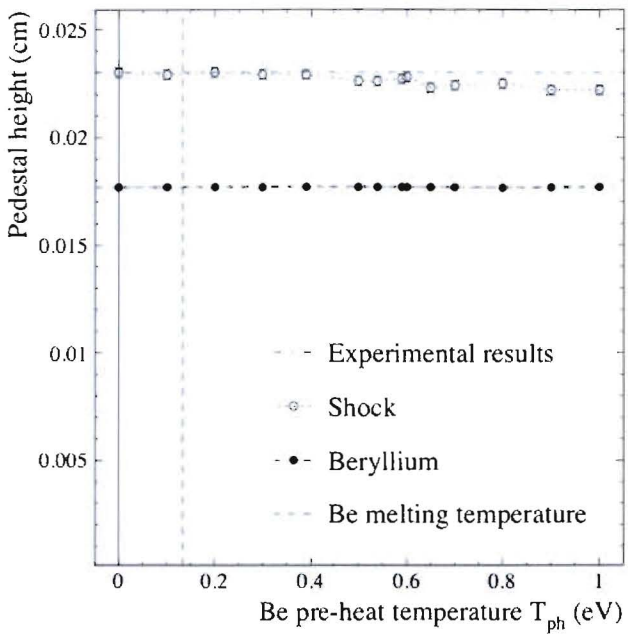
Pedestal height (cm)
0.025
0.02
0.015
0.01
0.005
0
0.2
0.4
0.6
0.8
1
Be pre-heat temperature T_{ph} (eV)
Experimental results
Shock
Beryllium
Be melting temperature

Figure 5

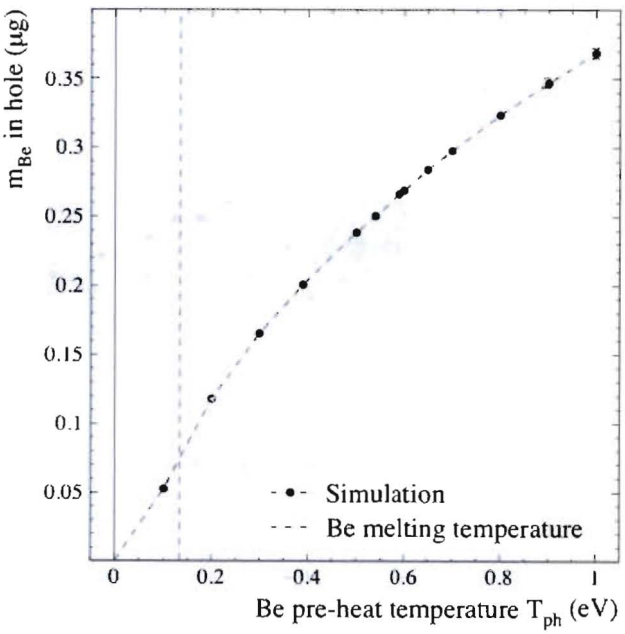
m_{Be} in hole (μg)
0.35
0.3
0.25
0.2
0.15
0.1
0.05
0
0.2
0.4
0.6
0.8
1
Simulation
Be melting temperature
Be pre-heat temperature T_{ph} (eV)

Figure 6

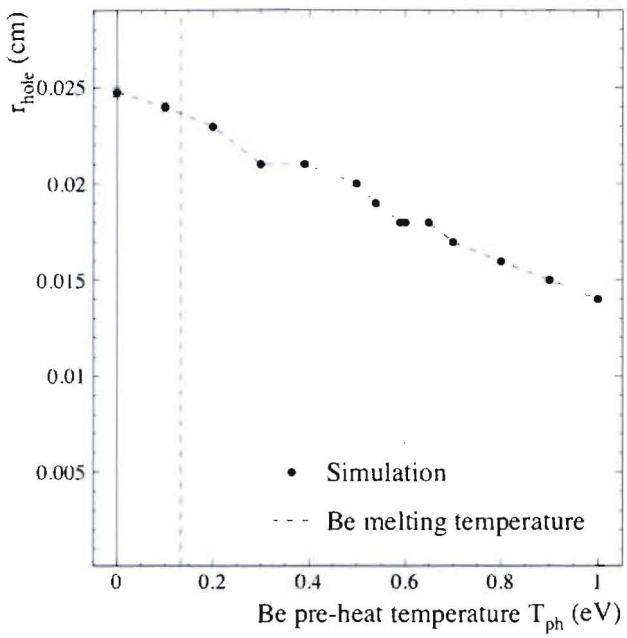
r_{hole} (cm)
0.025
0.02
0.015
0.01
0.005
Simulation
Be melting temperature
0
0.2
0.4
0.6
0.8
1
Be pre-heat temperature T_{ph} (eV)

Figure 7

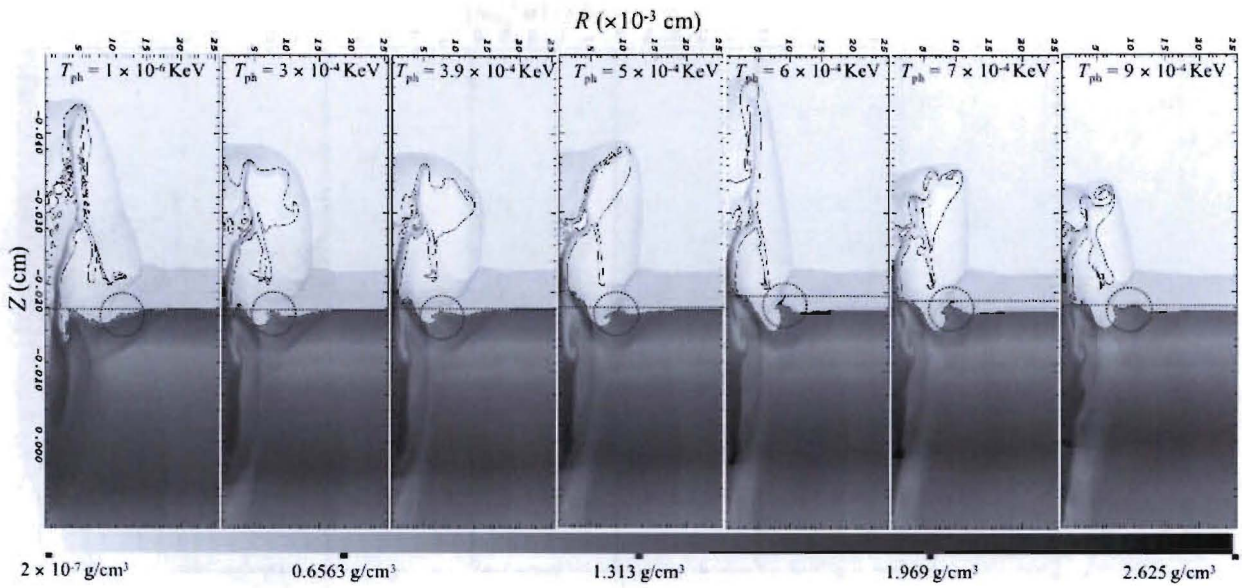
R (×10-3 cm)
Tph = 1 × 10-6 KeV
Tph = 3 × 10-4 KeV
Tph = 3.9 × 10-4 KeV
Tph = 5 × 10-4 KeV
Tph = 6 × 10-4 KeV
Tph = 7 × 10-4 KeV
Tph = 9 × 10-4 KeV
Z (cm)
2 × 10-7 g/cm3
0.6563 g/cm3
1.313 g/cm3
1.969 g/cm3
2.625 g/cm3

Figure 8

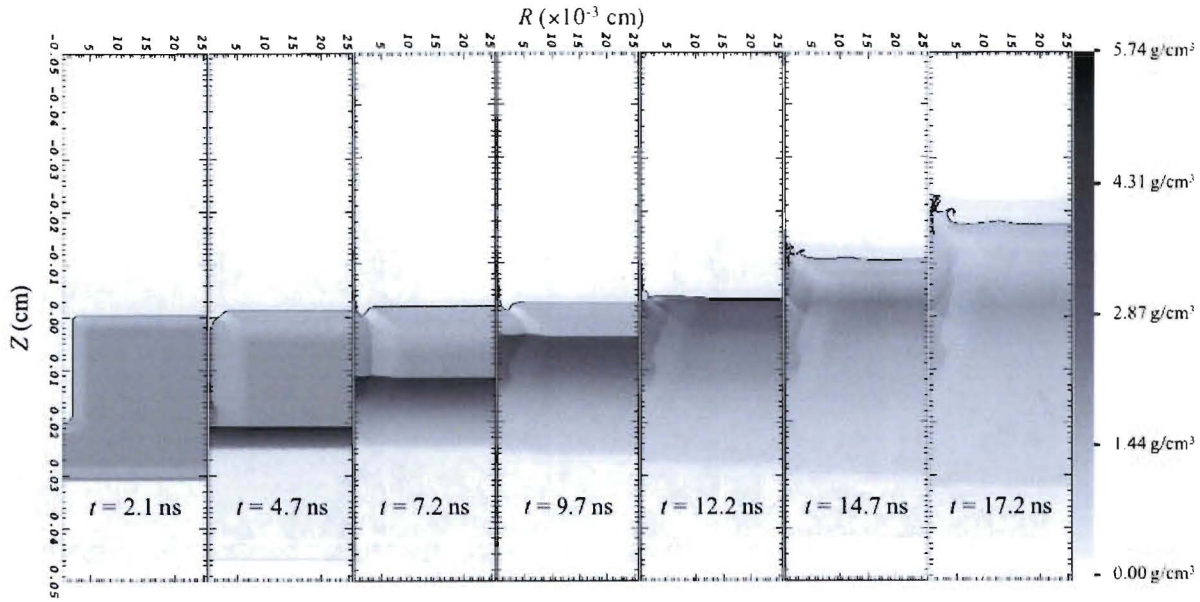
R (×10⁻³ cm)
Z (cm)
5.74 g/cm³
4.31 g/cm³
2.87 g/cm³
1.44 g/cm³
0.00 g/cm³
t = 2.1 ns
t = 4.7 ns
t = 7.2 ns
t = 9.7 ns
t = 12.2 ns
t = 14.7 ns
t = 17.2 ns

Figure 9

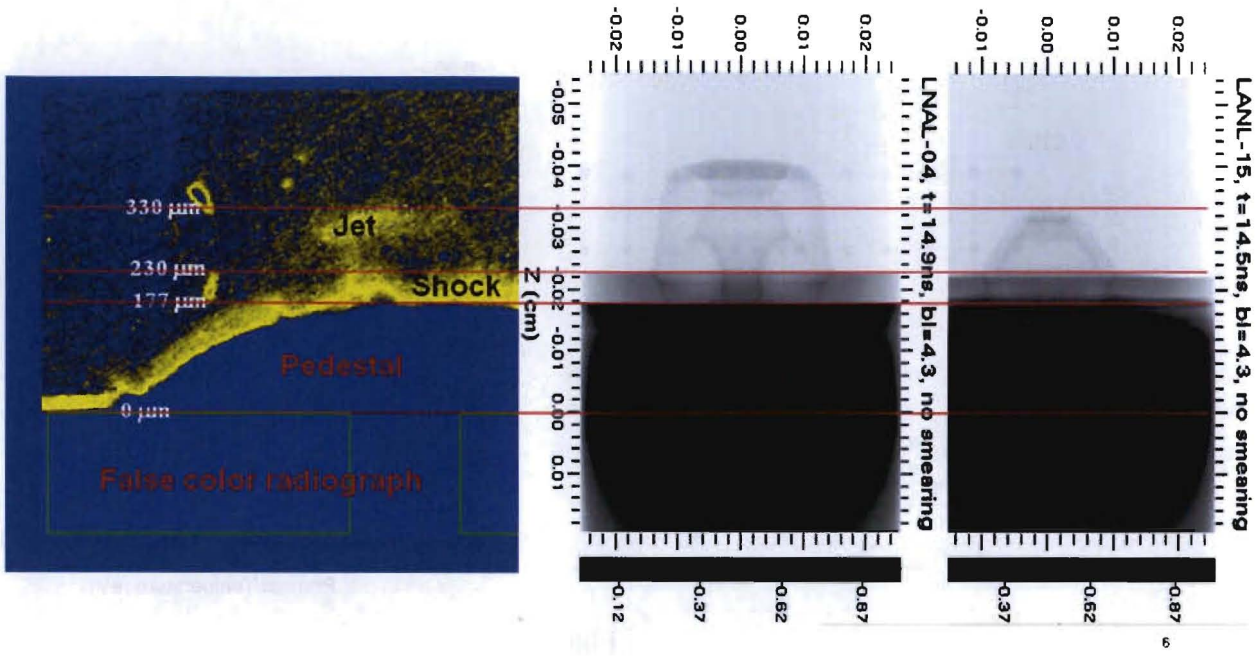
330 μm
230 μm
177 μm
0 μm
Jet
Shock
Pedestal
False color radiograph
Z (cm)
LANL-15, t=14.5ns, bl=4.3, no smearing
LNAL-04, t=14.9ns, bl=4.3, no smearing

Figure 10

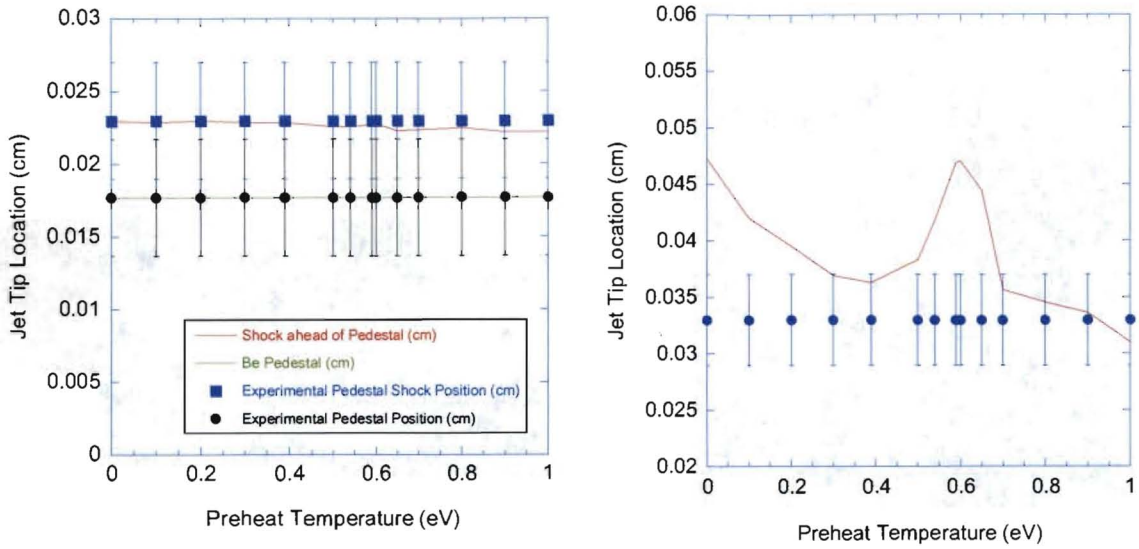
0.03
0.025
0.02
0.015
0.01
0.005
0
Jet Tip Location (cm)
0
0.2
0.4
0.6
0.8
1
Preheat Temperature (eV)
Shock ahead of Pedestal (cm)
Be Pedestal (cm)
Experimental Pedestal Shock Position (cm)
Experimental Pedestal Position (cm)
0.06
0.055
0.05
0.045
0.04
0.035
0.03
0.025
0.02
Jet Tip Location (cm)
0
0.2
0.4
0.6
0.8
1
Preheat Temperature (eV)

Figure 11

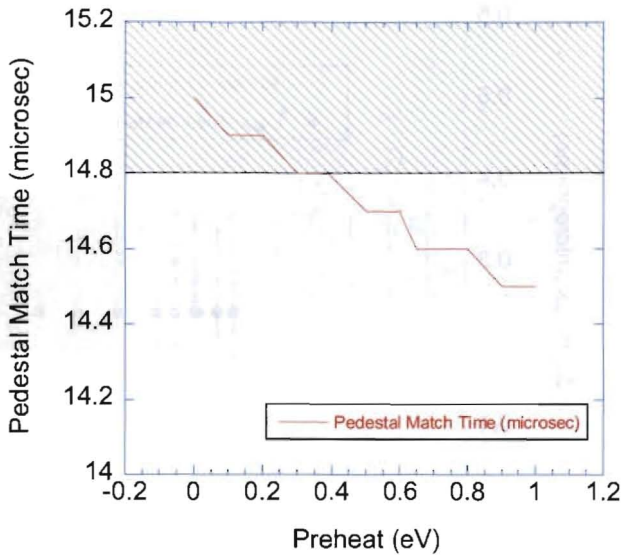
15.2
15
14.8
14.6
14.4
14.2
14
Pedestal Match Time (microsec)
-0.2
0
0.2
0.4
0.6
0.8
1
1.2
Preheat (eV)
Pedestal Match Time (microsec)

Figure 12

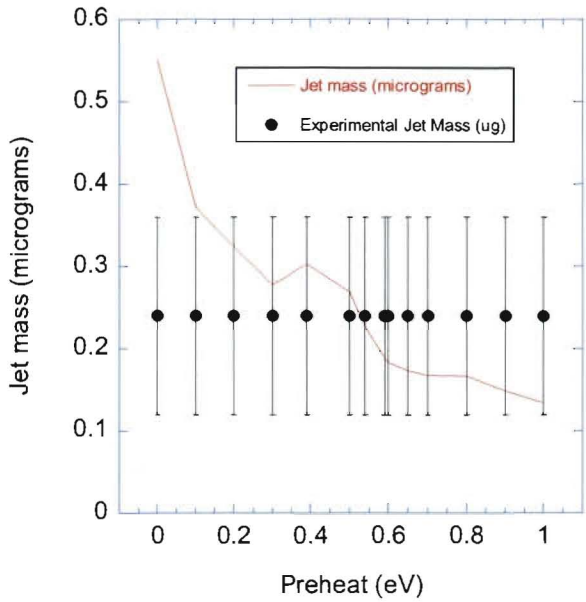
Jet mass (micrograms)
Experimental Jet Mass (ug)
Jet mass (micrograms)
Preheat (eV)
0.6
0.5
0.4
0.3
0.2
0.1
0
0
0.2
0.4
0.6
0.8
1

Figure 13

Figure 1: Cartoon of the experimental configuration. A laser drive heats a hohlraum, which radiatively ablates the BeCu ablator. This produces a shock which propagates into the washer and causes the material to form a jet in the vacuum region. This jet propagates into the foam where it is diagnosed.

Figure 2: A schematic of the initial configuration of the model, not to scale. See text for more detail. The temperature source is incident from the right.

Figure 3: The mass of the beryllium jet M_{jet} as a function of beryllium pre-heat temperature T_{ph} in KeV at time t ns. Error bars are estimated to be ten percent of the value of M_{jet}. A dashed line connects the results to guide the eye. The horizontal solid (dotted) line(s) shows the mean (errors on the) experimental results. The vertical dashed line shows the melting temperature of beryllium. Note the "shoulder" for 0.3 eV <= T_{ph} <= 0.6 eV. The shoulder is an artifact arising from the method used to determine M_{jet}. See text for details.

Figure 4: The height of the jet in cm as a function of beryllium pre-heat temperature T_{ph} in KeV at time t ~ 15 ns. Open circles show the height of the bow shock, dotted lines join the data points to guide the eye. Closed circles show the height of the beryllium jet, dashed lines join the data points to guide the eye. The horizontal dash-dotted line shows the experimental result. The vertical dashed line shows the melting temperature of beryllium.

Figure 5: The height of the pedestal in cm as a function of beryllium pre-heat temperature T_{ph} in KeV at time t ~ 15 ns. Open circles show the height of the shock, dotted lines join the data points to guide the eye. Closed circles show the height of the beryllium pedestal, dashed lines join the data points to guide the eye. The horizontal dash-dotted lines show the experimental results. The vertical dashed line shows the melting temperature of beryllium.

Figure 6: The mass of copper doped beryllium m_{Be} that has flowed into the cavity as a function of the initial temperature of the copper doped beryllium T_{ph} at the time when the shock due to the temperature source arrives at the bottom of the cavity. Dashed lines connect the data points to guide the eye. The vertical dashed line shows the melting temperature of beryllium.

Figure 7: The radius of the cavity r_{cavity} as a function of the initial temperature of the copper doped beryllium T_{ph} at the time when the shock due to the temperature source arrives at the bottom of the cavity. Dashed lines connect the data points to guide the eye. The vertical dashed line shows the melting temperature of beryllium.

Figure 8: The beryllium jet at time t ~ 15ns for the simulations which give rise to the "shoulder" shown in Figure 3. The gray scale shows the density of the materials. The solid line shows the interface between the CRF (top) and the copper doped beryllium (bottom). The dashed line shows the cut off boundary which defines the jet: any copper doped beryllium above the dashed line is considered part of the jet. The circles highlight a portion of the pedestal that changes the position of the cut off boundary. See text for further discussion. Also evident is the "peak" in jet height shown in Figure 4. As the initial temperature of the copper doped beryllium is increases the height of the jet increases until T_{ph} = 0.6 eV, thereafter the height of the jet decreases with increasing initial temperature of the copper doped beryllium. See text for further discussion

Figure 9: The simulation with an initial temperature of the copper doped beyrllium of T_{ph} = 0.9 eV at various times. The gray scale shows the density of the materials. The solid line shows the interface between the CRF (top) and the copper doped beryllium (bottom). A uniform shock is produced by pre-heating the copper doped beryllium to a temperature of T_{ph} = 0.9 eV and delaying the temperature source by 2.1 ns. At late times there is still a beryllium jet, but its height is less than the height of the shock wave ahead of the pedestal.

Figure 10: A comparison between the experimental results (left) and simulation results with no preheat (middle) and 0.7 eV of preheat (right). The simulation with preheat matches the data much more closely than the simulation without preheat.

Figure 11: A comparison of the experimentally pedestal (circles) and shock position (squares) and the simulation results. The simulations agree with the data quite well.

Figure 12: A blow up of the pedestal position match time in the simulations (curve) and the experimentally determined time of measurement including uncertainty (hatched region).

Figure 13: A comparison of the experimental determined jet mass (dots) and the simulated jet mass as a function of preheat level. There is agreement over a large range of preheat values.

[1] S. W. Haan, P.A. Amendt, T.R. Dittrich, *et al.*, Nucl. Fusion, **44**, S171, (2004).

[2] D. C. Wilson, P.A. Bradley, N.M Hoffman, *et al.*, Phys. Plasmas, **5**, 1953 (1998).

[3] D. C. Wilson, P.A. Bradley, S.R. Goldman, N.M Hoffman, R.W. Margevicius, R.B. Stephens and R.E. Olson, Fusion Technol, **38**, 16 (2000).

[4] J. Edwards, M. Marinak, T. Dittrich, S. Haan, J. Sanchez, J. Klingmann and J. Moody, Phys. Plasmas, **12**, 056318, (2005).

[5] G. R. Bennett, M.C. Herrmann, M.J. Edwards, *et al.*, Phys Rev Lett, **99**, 205003 (2007).

[6] S.H. Langer, N. Izumi, T.R. Dittrich and S.W. Haan, High Energy Density Physics, **3**, 169-174 (2007).

[7] J. M. Foster, B.H. Wilde, P.A. Rosen, *et al*, The Astrophysical Journal, **634**, L77-80 (2005).

[8] B. E. Blue, S.V. Weber, S.G. Glendinning, *et al*, Phys. Rev. Lett., **94**, 095005 (2005).

[9] T. R. Boehly, D.L. Brown, R.S Caxton, *et al*, Opt. Commun., **133**, 495 (1997).

[10] E. L. Dewald, K. M. Campbell, R. E. Turner, *et al.*, Rev. Sci. Instrum. **75**, 3759 (2004).

[11] http://physics.nist.gov/PhysRefData/Xcom/Text/XCOM.html

[12] N. E. Lanier, J. S. Cowan and J. Workman, Rev. Sci. Instrum, **77**, 043504 (2006).

[13] G. A. Kyrala, Rev. Sci. Instrum, **77**, 055104 (2006).

[14] M. M. Marinak, G.D. Kerbel, N.A. Gentile, O. Jones, D. Munro, S. Pollain, T.R. Dittrich and S.W. Haan, Phys. Plasmas 8, 2275 (2001).

[15] R.E. Olson, R. J. Leeper, A. Nobile, and J. A. Oertel, Phys. Rev. Lett., **91**, 235002-1 (2003).